

New Retinex Model-Based Infrared Image Enhancement

Thaweesak Trongtirakul^{*a}, Sos Agaian^b

^aDept. of Electrical Engineering, Faculty of Industrial Education, Rajamangala University of Technology Phra Nakhon, 399 Samsen Rd. Dusit Bangkok THAILAND 101300;

^bGraduate Center, City University of New York, 365 Fifth Ave., New York, NY USA 10016

ABSTRACT

The thermal imaging system often suffers from low contrast, low-spatial resolution, and blur under heat radiation conditions. Currently, available image enhancement methods are most suitable for visible images. However, existing methods often enhance objects and noise for noisy infrared images, simultaneously producing a very poor result. This paper presents two single infrared image enhancement methods, including (i) a Bi-Logarithmic Histogram Equalization with Quasi-symmetric correction and (ii) a combined luminance and reflection decomposition and image fusion-based method. Computer simulations on benchmarking infrared Kuangxd database show that the proposed algorithm performance outperforms conventional image enhancement methods, including a cutting-edge learning-based method, in terms of subjective and objective evaluations.

Keywords: Image Enhancement, Retinex, Thermal Imagery, Thermal Image Quality Assessment

1. INTRODUCTION

Recently, visual object detection, identification, and recognition remain core computer vision problems due to their wide application, including emotion identification, smart farming, mid-infrared spectroscopy, security monitoring, environment pollution detection, UAV imaging, driver-assist systems, photovoltaic inspection, remote sensing, infrared reflectography (applied to paintings on various mediums to reveal the under layers in a non-destructive manner), bio-medical, aerial photography, and other civil and military applications. Under good illumination conditions, considerable progress has been achieved in solving core computer vision problems. However, poor lighting conditions compromise its effectiveness. The low signal-to-noise ratio (SNR) drastically degrades the image quality in low light. Thermal images are superior to visible imaging because they can operate in darkness and tolerate illumination variations, which is one of the critical constraints of future autonomous systems.

Infrared sensors operate at wavelengths of 700 nm – 1.1 mm, which is longer than visible light (400 – 700 nm) [1]. Infrared imagery plays a vital role in military detection [2], surveillance, medical imaging [3, 4], oil spill applications [5], and visualization [6, 7]. Infrared has the advantage of low scattering and low lighting. However, infrared images also have some limitations, such as low contrast, lacking chrominance information, and blurred features, which restrict the capability to observe infrared targets and the advancement of infrared-based imaging applications. These difficulties make it difficult for infrared imaging applications to function effectively. It is crucial for numerous humanitarian applications of video analysis, including object detection, recognition, and visualization [8-10].

Visible imaging-based techniques have been widely applied to improve image quality, and the results are often good [11]. However, the effectiveness of cutting-edge techniques dramatically drops due to noise amplification and over- and under-enhancement. In this paper, we concentrate on the issues with visualization and image quality.

For all the reasons mentioned above, we aim to enhance the visual quality of infrared images in our work. We suggested a new framework for thermal image enhancement that primarily draws inspiration from Retinex decomposition and uses Image-Dependent Weighting Fusion (IDWF) of Histogram Equalization (HE)-based techniques. The proposed scheme comprises three key modules with post-processing tasks: Retinex decomposition, image enhancement, image fusion, and adaptive gamma correction. Additionally, grayscale-enhanced images are colored to illustrate the visual performance of images on pseudo-colors. Our work contributes in three ways:

1. We introduce a Bi-Logarithmic Histogram Equalization with Quasi-symmetric correction (BLHE-Q).
2. We offer a combined luminance and reflection decomposition and image fusion-based concept.
3. Extensive experiments are conducted on a publicly available dataset to illustrate that the proposed method is competitive with existing infrared image enhancement approaches.

The rest of the paper is organized as follows: Section II introduces the background of thermal-based image enhancement approaches. Then, our proposed technique for infrared images is presented in Section III. The computer simulation results are discussed in Section IV. Finally, the conclusion is given in Section V.

2. BACKGROUND

This section summarizes the existing techniques for improving the quality of an infrared image, from learning-free to learning-based methods. This overview also covers visible image enhancement techniques.

Infrared Radiation (IR) was discovered by Sir William Herschel in 1800 while studying radiation from the sun. Infrared (thermal imaging) is an advanced, non-invasive technology that uses infrared and thermal energy to collect objects' information by transforming infrared radiation (heat) into visible images displaying the spatial distribution of temperature differences in a thermal camera. Both thermal and infrared imaging allows us to "see" heat. The infrared region (IR) is divided into three classes: the near-infrared (NIR) (714–2,500 nm), the mid-infrared (MIR) (2,500–25,000 nm), and the far-infrared region (25,000–1×106 nm) [International Commission on Illumination (CIE)]. The margins between the three are inconsistent within the literature and practice and are defined by detector responses. The infrared region is also classified into five categories [11]:

1. *Near Infrared* (NIR): The near-infrared spectrum is located after the red wavelength. Typical application: night vision devices such as night vision goggles, infrared reflectography, and near-infrared spectroscopy.
2. *Short Wavelength Infrared* (SWIR): SWIR images are comparable to visible (black-and-white) images in detail and resolution. Typical application: long-distance telecommunications.
3. *Mid-Wavelength Infrared* (MWIR): The MWIR is also referred to as "thermal infrared" since radiation is emitted from the object itself, and no external light source is essential to image it. Application: it is used to guide missile technology. MWIR cameras are employed when the primary goal is to obtain high-quality images rather than focusing on temperature measurements and mobility.
4. *Long Wavelength Infrared* (LWIR): (LWIR temperature is slightly higher than room temperature. Application: "Thermal imaging" is used to detect thermal emissions from humans, vehicles, and animals.
5. *Far Infrared* (FIR): Application: it is used in far-infrared laser applications.

A. Learning-Free Methods: thermal-based images generally suffer from low-contrast, low-spatial resolution, noisy, and blurred information[12]. To solve these problems, conventional methods applied for visible images have been adopted to enhance infrared images. Among these methods, Histogram Equalization (HE) [13] is an important tool that increases the global contrast of images. HE has been employed either in a linear distribution form or in an extended one. For instance, HE method has been proposed to improve global contrast. Also, Contrast Limited Adaptive Histogram Equalization (CLAHE) utilizes HE-based methods to adjust local contrast. It is introduced to illustrate satisfactory hidden information and to control the degree of image enhancement. However, these two methods mentioned above generate over-contrast and over-brightness artifacts. To deal with these issues, the entire image was separated into several sub-images [14-21]. It is also known as "*Bi-Histogram Equalization (BHE)*." Kim used the threshold calculated by an image-dependent mean brightness value [14]. Later, Chen *et al.* minimized the Absolute Mean Brightness Error (AMBE) between an input image and an output image by optimizing an image-dependent threshold [15, 16]. Extended versions of BHE [17-20] simultaneously exploit different thresholds to control contrast and brightness. These techniques are suitable for improving global contrast and preserving overall brightness, but they suffer from a shortage of optimal brightness and contrast. BHE [14-20] calculates new intensity levels based on a linear distribution function. It is challenging to improve contrast when the histogram of an input image is fully distributed.

Retinex model is a non-linear image enhancement method that separates the entire image into two imaging components: reflectance and luminance. The reflectance component, $R_{i,j}$, represents the amount of illumination reflected by the object in the image and the luminance component, $L_{i,j}$, refers to the amount of illumination projected on the object in the image. Retinex-based methods can be classified into two categories: Single-Scale Retinex (SSR) and Multi-Scale Retinex (MSR). SSR [22, 23] convolves the neighbor function to generate the luminance component from an input image on a logarithmic domain. It creates remarkable scenes at under-exposed intensities. Jobson *et al.* [24] tested the logarithmic ratios between i) the image and a weighted average of an image; and ii) the image and a weighted product. These values are to choose between an altimetric mean and a geometric mean. Results visually confirm that images are better than the logarithmic function. For another Retinex-based model, MSR [25] uses a weighted sum of SSR output with multiple scales to provide color constancy and dynamic range. The weights are

changed to adjust color rendition and dynamic range compression. In general, small, medium, and large scales are adequate to enhance images.

B. Learning-Based Methods: Deep learning-based methods have recently demonstrated excellent performance in several computer and machine vision applications. It plays an important role in image classification, target detection, scene visualization, and pattern recognition. Deep learning architectures have been used in certain recent image enhancement techniques to improve the visual quality of visible and infrared images. Dong *et al.* [26] proposed the end-to-end learning method for mapping between low- and high-resolution images. The basic concept consists of a mapping deep Convolution Neural Network (CNN) that brings a low-resolution image as an input image and a high-resolution one as an output. Later, Kim *et al.*, [27] presented a highly accurate, Very Deep single-image Super-Resolution (VDSR) method based on VGG-net [28]. The VDSR method has become one of the most well-known CNN methods for image enhancement, improving the spatial resolution of visible images.

The majority of the existing methods for image enhancement in color domains focus on improving the spatial resolution of images. Few research papers for infrared image enhancement that cover other aspects such as low-contrast, blur boundaries, and denoise have been conducted. Thermal image Enhancement using CNN (TEN) [29] was proposed to transform a single low-resolution image into the applicable high-resolution image. Lee *et al.* also proposed a residual learning architecture [30] based Thermal Image Enhancement Convolution Neural Network (TIECNN) [31] that was inspired by mapping a low-to-high resolution approach. TIECNN outperforms traditional learning-based approaches for thermal-based image enhancement regarding training time complexity. In [32], Wang *et al.*, focused on improving infrared image quality. The network structure is improved by analyzing image characteristics. Occasionally, the resulting images illustrated some noisy regions between target objects. Thuan *et al.* proposed Generative Adversarial Network (GAN)-based super-resolution method. It integrates a residual block-based model that can perform super-resolution on GAN for thermal images while improving visual edge details. Finally, Thermal Enhancement architecture based on GAN (TE-GAN) is proposed by [33]. The architecture consists of contrast enhancement, denoising tasks, and edge restoration. These different modules are merged into a single architecture. However, TE-GAN requires visible image datasets for a training task.

3. PROPOSED ALGORITHM

This section presents an image quality metrics definition, a novel image enhancement method for thermal images that build upon the Retinex model applied for the image enhancement task, as shown in Figure 1.

Thermal image quality metrics definition [8]: the field of image quality assessment (IQA) has been researched for many years. However, traditional methods of no-reference IQA are not suitable for evaluating the quality of thermal images because they are structured differently than visible light images. It is not effective to use under-exposed, properly exposed, and over-exposed images to assess the quality of images.

Block Distribution-Based Information Measure (BDIM) [8] is a type of no-reference thermal image quality assessment metric that measures the perceived quality of a thermal image related to Human Visual System (HVS) properties. BDIM considers block-based attributes such as local resolution, contrast, and sharpness.

$$BDIM_{i,j}(p, I) = \frac{1}{m \times n} \sum_{i=1}^m \sum_{j=1}^n \frac{1}{\left(\frac{[p_{min}]^{m,n}}{[p_{min}]^{m,n} + [p_{max}]^{m,n}} \right) \left(\frac{[I_{min}]_{i,j}^{m,n}}{[I_{min}]_{i,j}^{m,n} + [I_{max}]_{i,j}^{m,n}} \right)^2 + \varepsilon} \quad (1)$$

where p_{min} and p_{max} respectively denote the minimum probability density value and the maximum probability density value in each local tile $[m, n]$, $[I_{min}]_{i,j}^{m,n}$ and $[I_{max}]_{i,j}^{m,n}$ represent the minimum intensity value and the maximum intensity value in each local tile $[m, n]$, respectively, and ε refers to an offset value.

The Blind/Referenceless Image Spatial Quality Evaluator (BRIQUE) [34] is an image quality assessment metric used to measure an image's perceived quality without needing a reference image. It is based on HVS and considers factors such as blur, noise, and color distortion to calculate a score that reflects the overall quality of the image.

Perception-based Image Quality Evaluator (PIQE) [35] aims to measure an image's perceived quality from the perspective of HVS. It considers various factors that affect how the HVS interprets and processes an image, such as resolution, contrast, and sharpness.

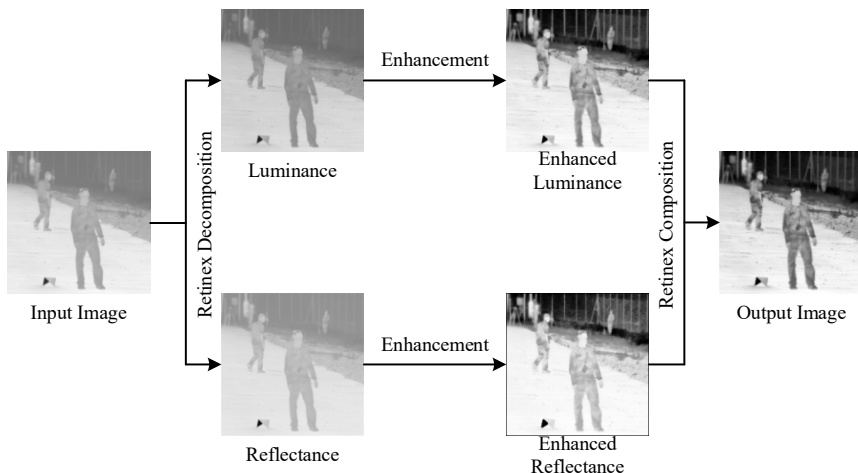


Figure 1 Retinex image enhancement scheme

The classic Retinex model proposed by Land and McCann is a computational model for estimating human color sensation. He named Retinex this system, and Retinex goals to reproduce the sensory response to color stimuli by the HVS color space. Retinex-based approaches have been explored for image enhancement. A simplified Retinex model involves decomposing an observed image $S_{i,j}$ into the reflectance component, $R_{i,j}$, and luminance component, $L_{i,j}$:

$$S_{i,j} = R_{i,j} \cdot L_{i,j} \quad (2)$$

$$R_{i,j} = \beta \log(\alpha S_{i,j} + c) - \log(F_{m,n} \otimes S_{i,j} + c) \quad (3)$$

where $F_{m,n}$ represents an imaging filter, c refers to an offset value, α and β respectively, denote a constant, \otimes is a convolution operator and where the illumination $L_{i,j}$, which is piece-wisely smooth, expresses the color of the light hitting the surfaces of objects in the scene $S_{i,j}$, while the reflectance R reflects the present physical characteristics of the observed scene $S_{i,j}$.

Nevertheless, Retinex decomposition is a highly ill-posed problem. Additionally, Retinex's composition, $Y_{i,j}$, the Retinex concept uses to improve the input image quality by increasing the visibility of its content and details, enhancing its colorfulness, and removing, some undesired effects of the illumination. The limitation is that when the illumination sharply changes, information in complex regions is not suitably illustrated and blurred, or luminance and reflectance cannot be accurately composed[36]. To resolve these issues, the reflectance function must be more accurately enhanced. The composition of Retinex can be expressed by:

$$Y_{i,j} = L_{i,j} \cdot R_{i,j}^2 \quad (4)$$

Image decomposition using Agaian-Trongtirakul Entropy (KL^2 Entropy) [10]: In this section, we decompose an image into dark and bright regions Based on KL^2 , We define the Extended Kapur Entropy, as:

$$x_\tau = \arg \max_x \{a(x) + b(x)\} \quad (5)$$

where x_τ be a threshold of the image and assume that $x_\tau \in \{x_0, x_1, \dots, x_{L-1}\}$. $L=255$, and the input image is decomposed into two sub-images $I_L(x)$ and $I_U(x)$ separated by x_τ as:

$$a(x) = (I_L(x) + \varepsilon)^\gamma \cos(\log(\log(I_L(x) + \varepsilon))) ; I_L(x) = \{I_{i,j} | I_{i,j} \leq x_\tau\} \quad (6)$$

$$b(x) = (I_U(x) + \varepsilon)^\gamma \cos(\log(\log(I_U + \varepsilon))) ; I_U(x) = \{I_{i,j} | I_{i,j} > x_\tau\} \quad (7)$$

Note that $I_L(x)$ is consist of $\{x_0, x_1, \dots, x_\tau\}$ and $I_U(x)$ is consists of $\{x_{\tau+1}, x_{\tau+2}, \dots, x_{L-1}\}$, $I_{i,j}$ refers to a Retinex imaging component, and ε denotes an offset value.

BLHE-Q (Bi-Logarithmic Histogram Equalization) Image Enhancement Algorithm

Let $X_{i,j}$ be an input image and $\mathbf{h}(x)$ be the histogram of $X_{i,j}$ composed of L discrete grayscale levels refer to $\{x_0, x_1, \dots, x_{L-1}\}$. Denote by x_τ the KL^2 threshold of the image $X_{i,j}$ and assume that $x_\tau \in \{x_0, x_1, \dots, x_{L-1}\}$.

Based on the KL^2 threshold, the histogram of the given image is decomposed into two sub-histograms $h_L(x)$ and $h_U(x)$ as $\mathbf{h}(x) = h_L(x) \cup h_U(x)$ where $h_L(x) = \{\mathbf{h}(x) | \mathbf{h}(x) \leq x_\tau\}$ and $h_U(x) = \{\mathbf{h}(x) | \mathbf{h}(x) > x_\tau\}$. The pseudocode of BLHE-Q is presented as Algorithm 1.

Algorithm 1: Bi-Logarithmic Histogram Equalization with Quasi-symmetric correction (BLHE-Q)

1. Compute the KL^2 threshold.
2. Separate the histogram of the input image into two sub-histograms by using the threshold.
3. Find the cumulative density function of sub-histograms.

$$c_L(x) = \sum_{i=0}^{x_\tau} p_L(x) \text{ and } c_U(x) = \sum_{i=x_\tau+1}^{x_{L-1}} p_U(x)$$

where p_L and p_U denote a probability density function of a dark component and a bright component.

4. Equalize the dark component and the bright component.

$$f_L(x) = a_L(x_\tau - x_0)e^{(c_L(x) \ln(1 + \frac{1}{a_L}))} + x_0 \text{ and } f_U(x) = a_U(x_{L-1} - x_\tau)e^{(c_U(x) \ln(1 + \frac{1}{a_U}))} + x_\tau$$

where a represents a constant, $c_L(x)$ and $c_U(x)$ respectively denote the cumulative density function of the dark component and the bright component, and ε denotes an offset value.

5. Generate two new images using the Quasi-symmetric correction functions.

$$q_1(x) = \begin{cases} f_L^\gamma(x), & x \leq x_\tau \\ 1 - (1 - f_L(x))^\frac{1}{\gamma}, & x > x_\tau \end{cases} \text{ and } q_2(x) = \begin{cases} 1 - (1 - f_U(x))^\frac{1}{\gamma}, & x \leq x_\tau \\ 1 - (1 - f_U(x))^\frac{1}{\gamma}, & x > x_\tau \end{cases}$$

where γ denotes a gamma parameter.

6. Generate the following parameters using:

$$I_L = 0.1(m \times n) \text{ and } I_H = 0.9(m \times n)$$

where m and n are the size of the input image.

7. Fuse Quasi-symmetric corrected images.

$$Q(x) = \eta q_1(x) + (1 - \eta)q_2(x); \eta = \frac{I_H - I_L}{I_H + I_L}$$

8. Output the enhanced image.
-

Note: Quasi-symmetric correction functions: this function is proposed to overcome the inherent defects of the classical enhancement function, for instance, gamma correction functions.

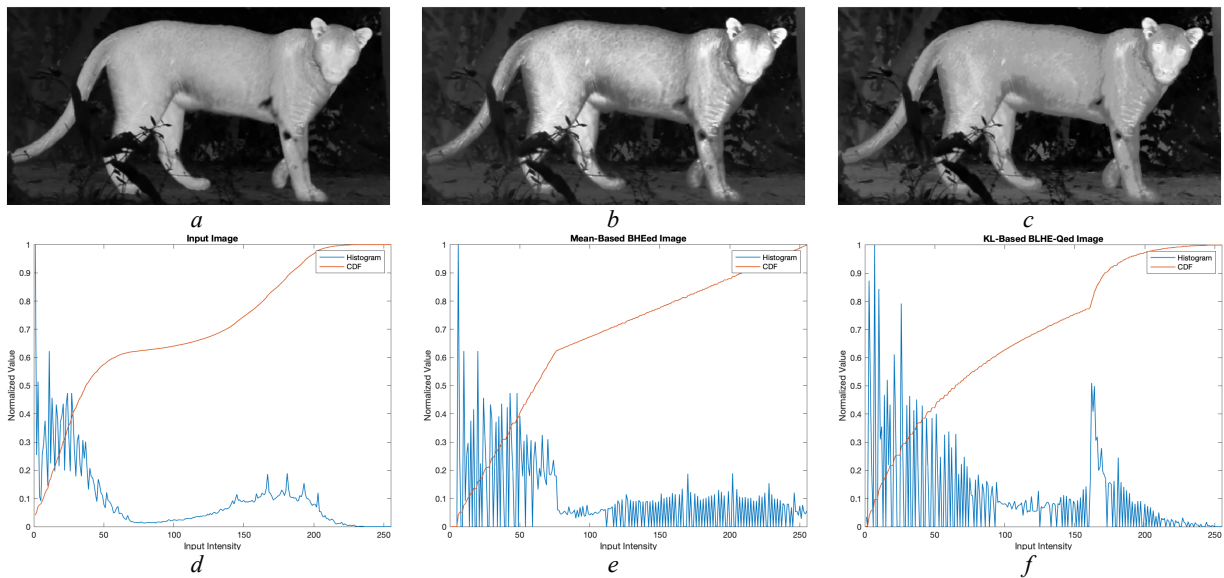


Figure 2 Comparison with different threshold-based mapping functions; a) input image, b) BHE separated by an image-dependent mean-based threshold, c) BLHE-Q separated by an image-dependent KL^2 -based threshold, d) histogram of the input image, and e) histogram of the BHEed image and f) histogram of the BLHE-Qed image

Based on Figure 2, classical BHE is effective in preserving overall brightness close to the input image. However, it generates over-enhanced regions, which result in artifacts and noise in the enhanced image. By contrast, BLHE-Q delivers satisfying results. The details are effectively enhanced.

Main Thermal Image Enhancement Algorithm (MTIEA): MTIEA is based on several histogram equalization methods, the Retinex decomposition theory, and an adaptive gamma correction algorithm. To increase more details on the Retinex imaging components, the proposed image enhancement procedures are illustrated in Algorithm 2, and the general concept is available in Figure 3.

Algorithm 2: Main Thermal Image Enhancement Algorithm (MTIEA)

1. Decompose an input image into illumination and reflection components using Retinex theory using Eq. 2-3.
2. Generate enhanced images (I_{BHE} , I_{CLAHE} , and I_{BLHE-Q}) by applying Bi-Histogram Equalization (BHE) [14], Contrast Limited Adaptive Histogram Equalization (CLAHE) [37], and Bi-Logarithmic Histogram Equalization with Quasi-symmetric correction (BLHE-Q) to the decomposed images: illumination and reflection.
3. Generate the thermal image quality-weighting map by calculating a frequency response map.

$$h_{m,n}(f_0, f) = F(\Omega_{m,n})$$
$$\Omega_{m,n}(\omega_0, \omega) \Big|_{\omega_0=\frac{22.26\pi}{60}, \omega=\frac{2\pi f}{60}} = e^{4\omega^2} (e^{-0.75} - 1) \cdot \frac{e^{8(\omega-\omega_0)} \cos^4(2\theta) + 1}{e^{8(\omega-\omega_0)} + 1}$$

where F represents a two-dimensional filter with the frequency response $\Omega_{m,n}(\omega_0, \omega)$, $\theta = \tan^{-1}\left(\frac{u^T}{u+c}\right)$, $u = [-20, 19, \dots, 20]$, and c denotes an offset value.

4. Determine a thermal image visualization operator [38].

$$BDIM_{i,j}(p, I) = \frac{1}{\left(\frac{[p_{min}]^{m,n}}{[p_{min}]^{m,n} + [p_{max}]^{m,n}} \right) \left(\frac{[I_{min}]_{i,j}^{m,n}}{[I_{min}]_{i,j}^{m,n} + [I_{max}]_{i,j}^{m,n}} \right)^2 + \varepsilon}$$

where p_{min} and p_{max} respectively denote the minimum probability density value and the maximum probability density value in each local tile $[m, n]$, $[I_{min}]_{i,j}^{m,n}$ and $[I_{max}]_{i,j}^{m,n}$ represent the minimum intensity value and the maximum intensity value in each local tile $[m, n]$, respectively, and c refers to an offset value.

5. Convolute the thermal image visualization operator with the frequency response map.
 $w = BDIM_{i,j} \otimes h_{m,n}$ where \otimes is a convolution operator.
6. Fuse enhanced images with thermal image quality metrics.

$$F_{i,j} = \sum_{\delta=1}^{\rho} W_{\delta} E_{i,j,\delta}; W_{\delta} = \frac{w_{\delta}}{\sum_{\delta=1}^{\rho} w_{\delta}}$$

where $w_{(\cdot)}$ represents a weighting image-dependent thermal image quality metric, $E_{i,j,(\cdot)}$ denotes an enhanced image using different image enhancement approaches, and ρ refers to the total number of enhanced images.

7. Apply an adaptive gamma correction.

$$J_{i,j} = x_{L-1} \left(\frac{F_{i,j}}{x_{L-1}} \right)^{\frac{\gamma x_{L-1}}{F_{i,j}}}$$

where γ represents a gamma correction parameter, x_{L-1} denotes the maximum intensity in a permitted intensity distribution range, and $F_{i,j}$ refers to a fused image.

8. Output the enhanced image.
-

4. COMPUTER SIMULATION RESULTS

In this section, the establishment of an infrared test dataset is detailed. Then, the resulting combination of different enhanced images is evaluated by a qualitative evaluation. Finally, the proposed results are compared with other cutting-edge enhancement algorithms objectively and subjectively. The implementation is programmed on MATLAB® 2022 and runs on a Readon Pro 570X 4GB GPU. The gamma parameter γ is set to 0.30.

Testing Dataset: We test the performance of the proposed method both qualitatively and quantitatively using the benchmarking dataset [39]. The dataset contains 16 images provided by Kuang *et al.* with a spatial resolution of 256×256 pixels.

Return to the Manage Active Submissions page at <http://spie.org/submissions/tasks.aspx> and approve or disapprove this submission. Your manuscript will not be published without this approval. Please contact authorhelp@spie.org with any questions or concerns.

Effect of the fusion with different enhanced images: we investigate the impact of the imaging combination. The first fusion of BHEed and CLAHEed images illustrates a great informative scene but shows a noisy background. The second fusion of BHEed and BLHE-Qed images present the under-exposed background.

The third fusion of CLAHEed and BLHE-Qed images improves background information. The enhancement effect cleans up the details in bright regions and amplifies noise in dark regions. Finally, the fusion of the three enhanced images improves the contrast and informative features in the background and foreground. It tends not to be enhanced.

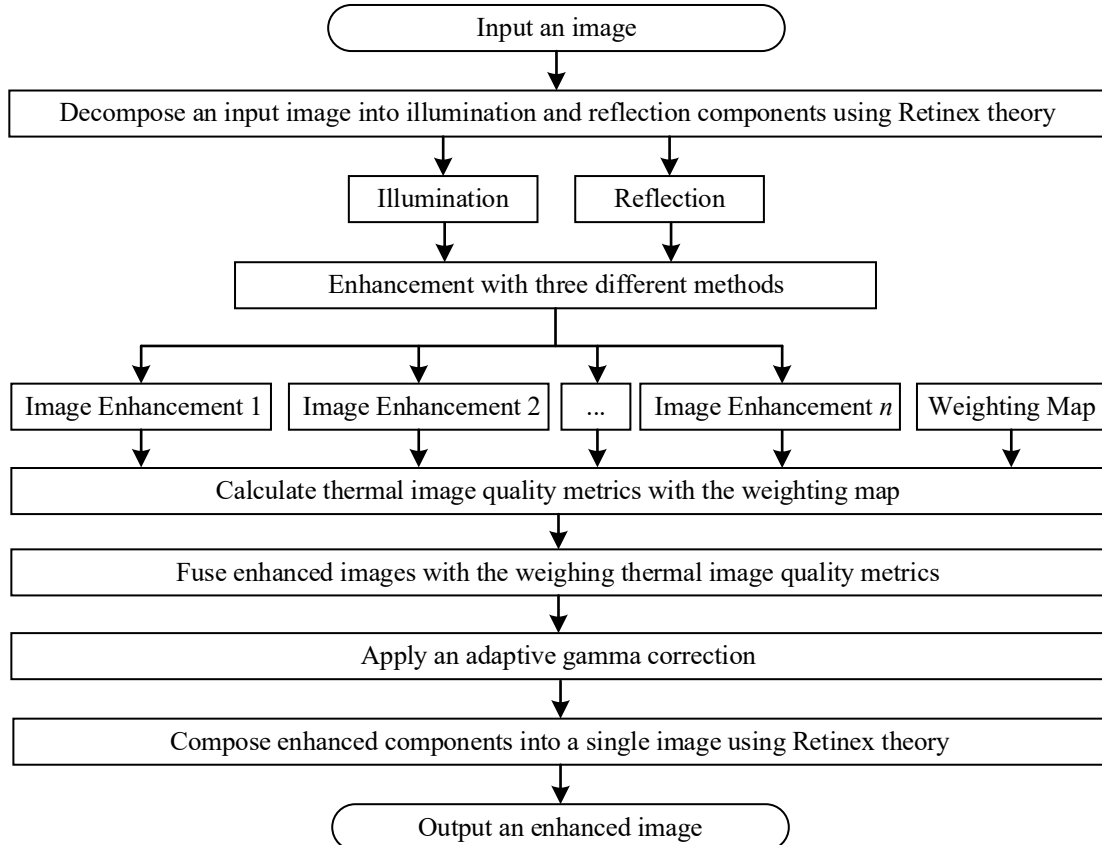


Figure 3 The concept of the combined luminance and reflection decomposition, and image quality measure-based image fusion

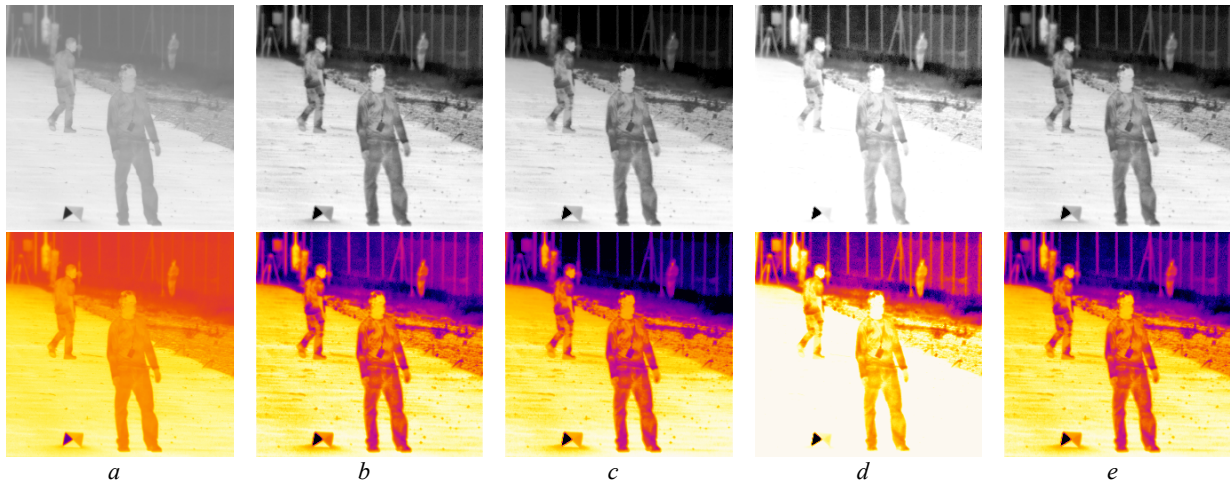


Figure 4 Comparison of the composition of enhancement; a) input image, b) fusion of BHE and CLAHE, c) fusion of BHE and BLHE-Q, d) fusion of CLAHE and BLHE-Q, e) fusion of BHE, CLAHE, and BLHE-Q

Evaluation Metrics: Blind/Referenceless Image Spatial Quality Evaluator (BRISQUE), Perception-based Image Quality Evaluator (PIQE), and Block-Distribution-based Information Measure (BDIM) are used as the evaluation metrics. The higher values illustrate the improved enhancement performance.

Comparison with existing methods: the performance of the proposed method is compared with two conventional histogram-based approaches and cutting-edge infrared image enhancement methods: Histogram Equalization (HE) [13], Contrast Limited Adaptive Histogram Equalization (CLAHE) [37] and Image Enhancement-Conditional Generative Adversarial Network (IE-CGAN) [39] which resulting images are available at: <https://github.com/Kuangxd/IE-CGAN>.

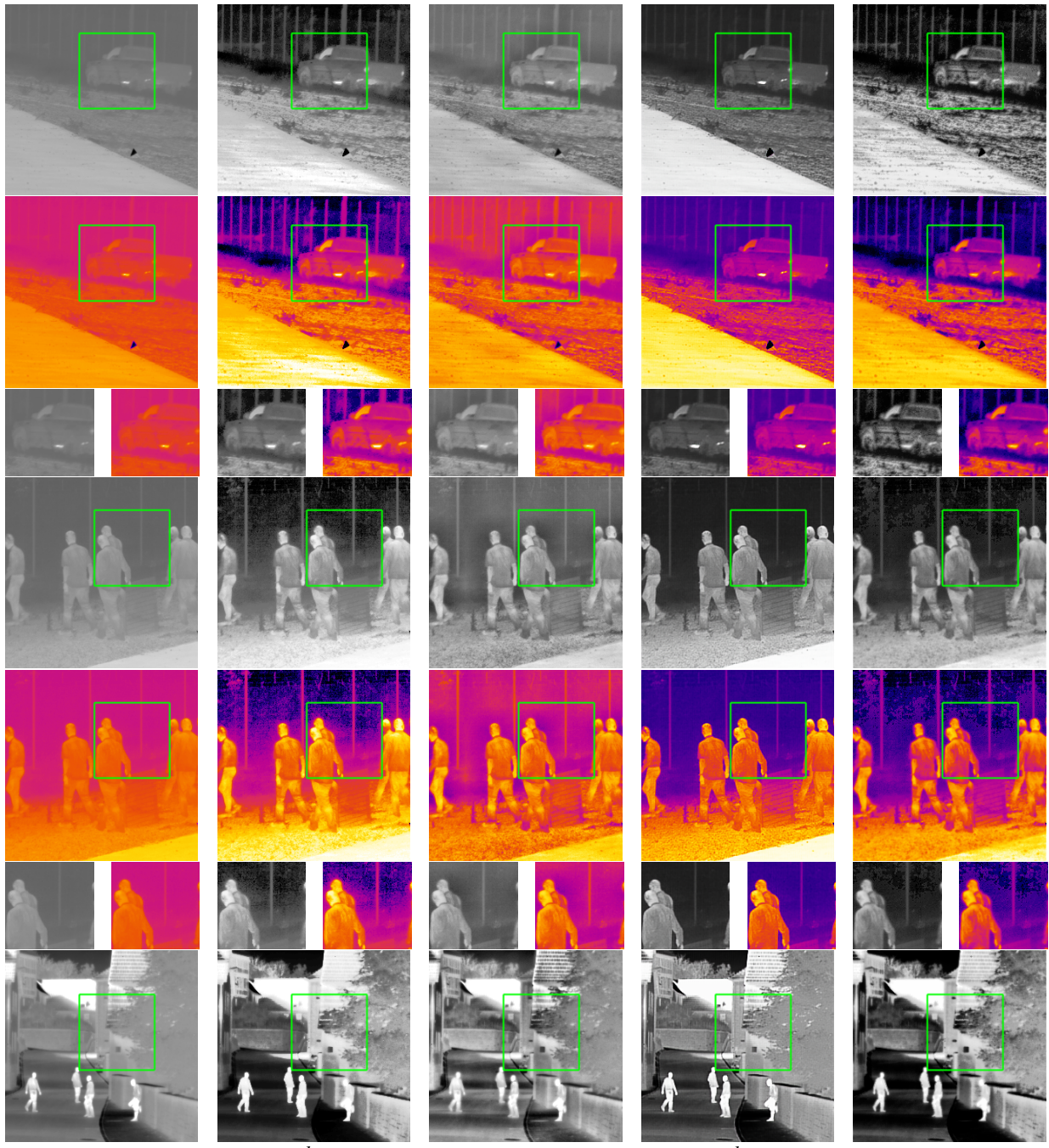


Figure 5 Results generated by different image enhancement methods; a) input low-contrast image, b) HE [13],
c) CLAHE [37], d) IE-CGAN [39], and e) the proposed method.

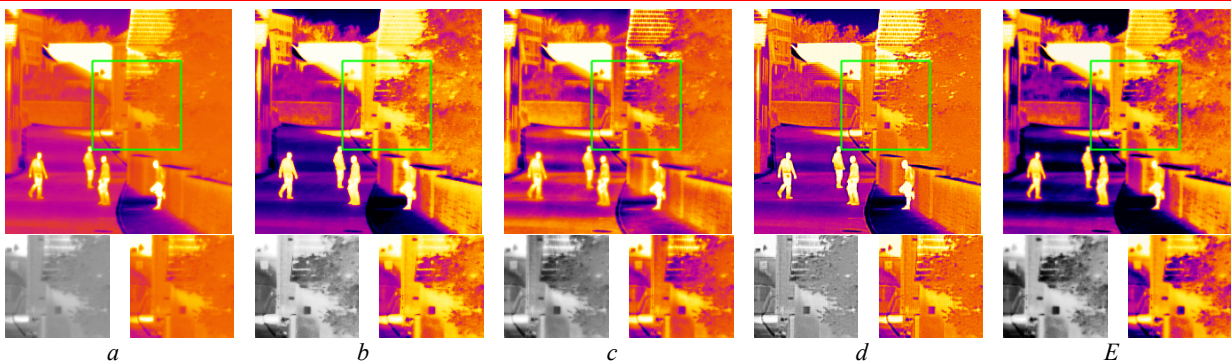


Figure 5(Cont.) Results generated by different image enhancement methods; *a*) input low-contrast image, *b*) HE [13],
c) CLAHE [37], *d*) IE-CGAN [39], and *e*) the proposed method

Qualitative Observation: we compare the performance of our proposed method and existing algorithms on the infrared dataset [39]. Figure 4 depicts the enhanced images of four low-contrast infrared images using different algorithms. Note that the HE leads to over-enhancement with noisy scenes while CLAHE leads to under-enhancement with a hazy artifact. The supervised approach, IE-CGAN, effectively eliminates the problem of over- and under-enhancement. However, the learning-based method washes out details on dark and bright regions. On the other hand, the proposed method can significantly reveal information and improve contrast while suppressing noise in various scenarios.

Table 1 Average results of BRIQUE, PIQE, and BDIM

Metric	HE [13]	CLAHE [37]	IE-CGAN [39]	Proposed
BRIQUE [34]	25.7212	23.9212	19.5826	31.5416
PIQE [35]	41.1011	28.9818	24.6357	43.4639
BDIM [8]	0.4733	0.3598	0.4215	0.6628

Quantitative Evaluation: we compare the proposed method with HE, CLAHE, and IE-CGAN methods on the infrared dataset. Simulation results are illustrated in Table 1. We can see that it achieves the highest scores across all evaluation metrics.

Advantages of the proposed enhancement method: we visually introduce the enhanced image on a noise-free image and the enhanced image on a noisy image of our proposed enhancement method, as shown in Figure 6. As an observation, the enhanced image of a noisy image using the proposed image enhancement method contains visible information resulting in high-contrast features. By subtracting between the enhanced noisy image and the enhanced noise-free image illustrated in Figure 6(*f*), our method produces a natural-looking denoised appearance.

The Multi-Scale Structural Similarity Measure (MS-SSIM) index for testing noisy and noise-free images is presented in Table 2. The first row shows the comparison of the input and noisy images, with an MS-SSIM value of 0.9992, indicating a slight alteration in the image's data structure. Similarly, the second row compares the imaging structure between the enhanced image and the noisy enhanced image, with a value of 0.9943, also demonstrating a slight change.

The MS-SSIM value of an input image and a noisy image added by Gaussian is presented in the first row. The value illustrates that the structural similarity of the noisy image is slightly changed (0.9992). Similarly, the structural similarity comparison between an enhanced image and an enhanced noisy image shows that the MS-SSIM is slightly changed (0.9943).

The results of the inter-class imaging structure comparison between an input image and the enhanced image illustrated that the MS-SSIM value is 0.6998, while the comparison between an input image and the enhanced noisy image is 0.6989. These values suggest a change in the imaging structure between the two images, as indicated by the improved visual clarity and increased details observed in the enhanced images depicted in Figure 6. It is worth noting that the MS-SSIM value for the enhanced noisy image is relatively close to that of the enhanced image with noise-free, indicating that the presence of our enhancement approach had a significant impact on reducing noises and preserving the overall imaging structure.

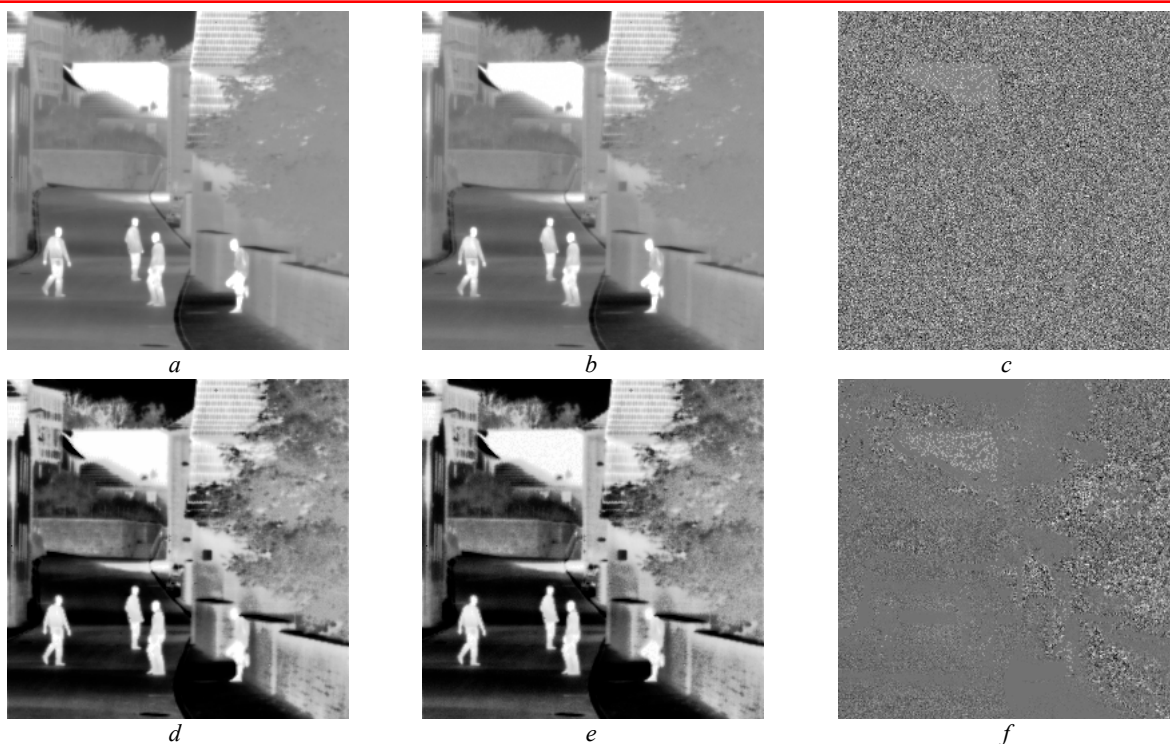


Figure 6 Illustrative enhanced image with noise removal; *a*) input image – noise free, *b*) noisy image – input image with Gaussian noise, *c*) Gaussian noise – the difference between the input image and the noisy image, *d*) enhanced image, *e*) enhanced noisy image, *f*) Gaussian noise reduced by the proposed enhancement – the difference between the enhanced image and the enhanced noisy image

Table 2 Structural comparison of the proposed method by using MS-SSIM on noisy and noise-free images

Image	Reference	MS-SSIM
Input image	Input image with Gaussian noise	0.9992
Enhanced image	Enhanced noisy image	0.9943
Enhanced image	Input image	0.6998
Input image	Enhanced image with Gaussian noise	0.6922
Input image	Enhanced noisy image	0.6989

5. CONCLUSION

In this paper, we proposed a new Retinex model-based infrared image enhancement for illuminance and reflectance decomposition. We first introduced the Agaian-Trontirakul Entropy (KL^2 entropy-based threshold) to partition the entire image into two sub-images. The decomposed images are enhanced by applying Bi-Histogram Equalization (BHE), Contrast Limited Adaptive Histogram Equalization (CLAHE), and Bi-Logarithmic Histogram Equalization with Quasi-symmetric correction (BLHE-Q). In addition, we proposed the BLHE-Q algorithm to produce a brightness-preserved and enhanced image. The enhanced images are combined with a thermal image visualization operator called “Block Distribution-Based Information Measure (BDIM)” for better fusion performance. Quantitative and qualitative assessments presented that the proposed method outperforms the competitive methods in contrast enhancement and noise removal simultaneously. The experimental results on the infrared dataset proved that our method could yield satisfactory enhanced images.

6. ACKNOWLEDGEMENT

This research partially was funded by the Coordinating Center for Thai Government Science and Technology Scholarship Students (CSTS), National Science and Technology Development Agency (NSTDA), Ministry of Higher Education, Science, Research, and Innovation under grant no. JRA-CO-2565-17450-TH.

REFERENCES

- [1] L. Xu, P. Liang, J. Han, L. Bai, and D. Z. Chen, "Global filter of fusing near-infrared and visible images in frequency domain for defogging," *IEEE Signal Processing Letters*, vol. 29, pp. 1953-1957, doi: 10.1109/LSP.2022.3205271.
- [2] H. Kaushal and G. Kaddoum, "Applications of lasers for tactical military operations," *IEEE Access*, vol. 5, pp. 20736-20753, doi: 10.1109/ACCESS.2017.2755678.
- [3] A. Hakim and R. N. Awale, "Thermal imaging - an emerging modality for breast cancer detection: a comprehensive review," *Journal of Medical Systems*, vol. 44, no. 8, p. 136, 1 July 2020, doi: 10.1007/s10916-020-01581-y.
- [4] T. Trongtirakul, A. Oulefki, S. Agaian, and W. Chiracharit, "Enhancement and segmentation of breast thermograms," in *Proc.SPIE*, vol. 11399, p. 113990F, doi: 10.1117/12.2554594.
- [5] A. Oulefki, T. Trongtirakul, S. Agaian, and W. Chiracharit, *Detection and visualization of oil spill using thermal images* (SPIE Defense + Commercial Sensing). SPIE.
- [6] T. Trongtirakul and S. Agaian, "Transmission map optimization for single image dehazing," presented at the Proc. SPIE 12100, Multimodal Image Exploitation and Learning 2022, 27 May 2022. [Online]. Available: 10.1117/12.2621831.
- [7] T. Trongtirakul and S. Agaian, "Adaptive inertia weight particle swarm algorithm for optimized hyperspectral image enhancement," in *Proc.SPIE*, vol. 11734, p. 1173403, doi: 10.1117/12.2585548.
- [8] T. Trongtirakul and S. Agaian, "Unsupervised and optimized thermal image quality enhancement and visual surveillance applications," *Signal Processing: Image Communication*, vol. 105, p. 116714, 1 July 2022, doi: 10.1016/j.image.2022.116714.
- [9] T. Trongtirakul, W. Chiracharit, and S. Agaian, "Color restoration of multispectral images: near-infrared (NIR) filter-to-color (RGB) image," presented at the Proc. IS&T Int'l. Symp. on Electronic Imaging: Image Processing: Algorithms and Systems XVIII, 2020.
- [10] S. B. e. al., "COVI3D: Automatic COVID-19 CT image-based classification and visualization platform utilizing virtual and augmented reality technologies," *Diagnostics*, vol. 12, no. 3, doi: 10.3390/diagnostics12030649.
- [11] R. Gaber, A. Ali, and K. Ahmed, "Performance evaluation of infrared image enhancement techniques," *ArXiv*, vol. abs/2202.03427.
- [12] L. Lu, Y. Zhou, K. Panetta, and S. Agaian, *Comparative study of histogram equalization algorithms for image enhancement* (SPIE Defense, Security, and Sensing). SPIE, 2010.
- [13] J. H. Han, S. Yang, and B. U. Lee, "A novel 3-D color histogram equalization method with uniform 1-D gray scale histogram," *IEEE Transactions on Image Processing*, vol. 20, no. 2, pp. 506-512, 2011, doi: 10.1109/TIP.2010.2068555.
- [14] Y. T. Kim, "Contrast enhancement using brightness preserving bi-histogram equalization," *IEEE Transactions on Consumer Electronics*, vol. 43, no. 1, pp. 1-8, doi: 10.1109/30.580378.
- [15] S. D. Chen and A. R. Ramli, "Preserving brightness in histogram equalization based contrast enhancement techniques," *Digital Signal Processing*, vol. 14, no. 5, pp. 413-428, 1 September 2004, doi: 10.1016/j.dsp.2004.04.001.
- [16] S. D. Chen and A. R. Ramli, "Minimum mean brightness error bi-histogram equalization in contrast enhancement," *IEEE Transactions on Consumer Electronics*, vol. 49, no. 4, pp. 1310-1319, doi: 10.1109/TCE.2003.1261234.
- [17] W. Yu, C. Qian, and Z. Baeomin, "Image enhancement based on equal area dualistic sub-image histogram equalization method," *IEEE Transactions on Consumer Electronics*, vol. 45, no. 1, pp. 68-75, doi: 10.1109/30.754419.
- [18] K. G. Dhal and S. Das, "Combination of histogram segmentation and modification to preserve the original brightness of the images," *Pattern Recognition and Image Analysis*, vol. 27, no. 2, pp. 200-212, 2017/04/01, doi: 10.1134/S1054661817020031.
- [19] N. Otsu, "A threshold selection method from gray-level histograms," *IEEE Transactions on Systems, Man, and Cybernetics*, vol. 9, no. 1, pp. 62-66, doi: 10.1109/TSMC.1979.4310076.
- [20] J. N. Kapur, P. K. Sahoo, and A. K. C. Wong, "A new method for gray-level picture thresholding using the entropy of the histogram," *Computer Vision, Graphics, and Image Processing*, vol. 29, no. 3, pp. 273-285, 1 March 1985, doi: 10.1016/0734-189X(85)90125-2.
- [21] T. Trongtirakul and S. Agaian, "Weighted histogram equalization using entropy of probability density function," arXiv, doi: 10.48550/arXiv.2111.08578.

- [22] K. Ngaiming *et al.*, "Single-scale center-surround Retinex based restoration of low-illumination images with edge enhancement," in *Proc. SPIE*, vol. 10615, p. 106152R, doi: 10.1117/12.2302614.
- [23] M. K. Ismail and Z. A. Ameen, "Adapted single scale Retinex algorithm for nighttime image enhancement," (in en), *AL-Rafidain Journal of Computer Sciences and Mathematics*, vol. 16, no. 1, pp. 59-69, 06/17, doi: 10.33899/csmj.2022.174407.
- [24] D. J. Jobson, Z. Rahman, and G. A. Woodell, "Properties and performance of a center/surround retinex," *IEEE Transactions on Image Processing*, vol. 6, no. 3, pp. 451-462, doi: 10.1109/83.557356.
- [25] Z. Mahmood, N. Muhammad, N. Bibi, M. M. Yasir, and N. Ahmed, "Human visual enhancement using multi scale Retinex," *Informatics in Medicine Unlocked*, vol. 13, pp. 9-20, 1 January 2018, doi: 10.1016/j.imu.2018.09.001.
- [26] C. Dong, C. C. Loy, K. He, and X. Tang, "Image super-resolution using deep convolutional networks," *IEEE Transactions on Pattern Analysis and Machine Intelligence*, vol. 38, no. 2, pp. 295-307, doi: 10.1109/TPAMI.2015.2439281.
- [27] A. Oulefki, S. S. Agaian, T. Trongtirakul, and A. K. Laouar, "Automatic COVID-19 lung infected region segmentation and measurement using CT-scans images," (in eng), *Pattern recognition*, vol. 114, pp. 107747-107747, 2021, doi: 10.1016/j.patcog.2020.107747.
- [28] K. Simonyan and A. Zisserman, "Very deep convolutional networks for large-scale image recognition," *CoRR*, vol. abs/1409.1556.
- [29] Y. Choi, N. Kim, S. Hwang, and I. S. Kweon, "Thermal image enhancement using convolutional neural network," in *IEEE/RSJ International Conference on Intelligent Robots and Systems (IROS)*, 9 October 2016, pp. 223-230, doi: 10.1109/IROS.2016.7759059.
- [30] J. Kim, J. K. Lee, and K. M. Lee, "Accurate image super-resolution using very deep convolutional networks," in *2016 IEEE Conference on Computer Vision and Pattern Recognition (CVPR)*, 27-30 June 2016, pp. 1646-1654, doi: 10.1109/CVPR.2016.182.
- [31] K. Lee, J. Lee, S. Hwang, and S. Lee, "Brightness-based convolutional neural network for thermal image enhancement," *IEEE Access*, vol. 5, pp. 26867-26879, doi: 10.1109/ACCESS.2017.2769687.
- [32] J. Wang and Y. Liu, "Infrared image super-resolution enhancement based on convolutional neural network," in *International Joint Conference on Information, Media and Engineering (IJCIME)*, 17 December 2019, pp. 272-275, doi: 10.1109/IJCIME49369.2019.00061.
- [33] M. A. Marnissi, H. Fradi, A. Sahbani, and N. E. B. Amara, "Thermal image enhancement using generative adversarial network for pedestrian detection," in *25th International Conference on Pattern Recognition (ICPR)*, 10-15 January 2021, pp. 6509-6516, doi: 10.1109/ICPR48806.2021.9412331.
- [34] A. Mittal, A. K. Moorthy, and A. C. Bovik, "No-reference image quality assessment in the spatial domain," *IEEE Transactions on Image Processing*, vol. 21, no. 12, pp. 4695-4708, 2012, doi: 10.1109/TIP.2012.2214050.
- [35] N. Venkatanath, D. Praneeth, B. M. Chandrasekhar, S. S. Channappayya, and S. S. Medasani, "Blind image quality evaluation using perception based features," in *Twenty First National Conference on Communications (NCC)*, 27 February - 1 March 2015 2015, pp. 1-6, doi: 10.1109/NCC.2015.7084843.
- [36] A. S. Parihar and K. Singh, "A study on Retinex based method for image enhancement," in *2nd International Conference on Inventive Systems and Control (ICISC)*, 19-20 January 2018, pp. 619-624, doi: 10.1109/ICISC.2018.8398874.
- [37] S. F. Tan and N. A. M. Isa, "Exposure based multi-histogram equalization contrast enhancement for non-uniform illumination images," *IEEE Access*, vol. 7, pp. 70842-70861, 2019, doi: 10.1109/ACCESS.2019.2918557.
- [38] S. Agaian, *Visual morphology* (Electronic Imaging '99). SPIE.
- [39] X. Kuang, X. Sui, Y. Liu, Q. Chen, and G. Gu, "Single infrared image enhancement using a deep convolutional neural network," *Neurocomputing*, vol. 332, pp. 119-128, 7 March 2019, doi: 10.1016/j.neucom.2018.11.081.